Nano Energy 56 (2019) 216–224

Contents lists available at ScienceDirect

Nano Energy

journal homepage: www.elsevier.com/locate/nanoen

Full paper

Flexible piezoelectric ultrasonic energy harvester array for bio-implantable wireless generator

Laiming Jiang[a,c], Yang Yang[b,*], Ruimin Chen[d], Gengxi Lu[d], Runze Li[a,d], Di Li[e], Mark S. Humayun[a], K. Kirk Shung[d], Jianguo Zhu[c,*], Yong Chen[b,*], Qifa Zhou[a,*]

[a] Roski Eye Institute, Keck School of Medicine, University of Southern California, Los Angeles, CA 90033, USA
[b] Epstein Department of Industrial and Systems Engineering, Department of Aerospace and Mechanical Engineering, Viterbi School of Engineering, University of Southern California, Los Angeles, CA 90089, USA
[c] College of Materials Science and Engineering, Sichuan University, Chengdu 610064, China
[d] Department of Biomedical Engineering, Viterbi School of Engineering, University of Southern California, Los Angeles, CA 90089, USA
[e] School of Microelectronics, Xidian University, Xi'an 710071, China

ARTICLE INFO

Keywords:
Flexible device
Ultrasonic energy harvester
Piezoelectric
Wireless generator

ABSTRACT

Ultrasonic driven wireless charging technology has recently attracted much attention in the next generation bio-implantable systems; however, most developed ultrasonic energy harvesters are bulky and rigid and cannot be applied to general complex surfaces. Here, a flexible piezoelectric ultrasonic energy harvester (PUEH) array was designed and fabricated by integrating a large number of piezoelectric active elements with multilayered flexible electrodes in an elastomer membrane. The developed flexible PUEH device can be driven by the ultrasonic wave to produce continuous voltage and current outputs on both planar and curved surfaces, reaching output signals of more than 2 Vpp and 4 μA, respectively. Potential applications of using the flexible PUEH to charge energy-storage devices and power commercial electronics were demonstrated. Its low attenuation performance was also evaluated using the in vitro test of transmitting power through pork tissue, demonstrating its potential use in the next generation of wirelessly powered bio-implantable micro-devices.

1. Introduction

Bio-implantable devices have recently attracted much interest due to their wide applications for millions of patients in various scenarios, such as high-density neural stimulation, cardioverter defibrillators, artificial retinas, pacemakers, etc. [1–3]. The advancements in current battery technology for bio-implantable devices have led to significant improvement in storage capacity and size reduction. However, the battery life is still limited to a few years and the surgeries for periodic replacement of the batteries will extend hospitalization time and expose patients to health risks such as high morbidity or even mortality [4,5]. The lifetime of batteries needs to be prolonged or an alternative technology that can eliminate the battery replacement from implants is required. Self-powered bio-implantable systems based on piezoelectric effect have been studied before that can to diminish the medical burden of replacements of batteries and costs for patients [6,7]. These systems integrate energy harvesting devices inside human body and generate electric power from periodical biomechanical movements (including muscle contraction/relaxation, cardiac/lung motions, and blood circulation) or external sources outside human body (e.g., inductive power transfer and acoustic energy transfer) [6,8]. Compared to the energy harvesting from internal organ movement, the external sources provide adaptable and stable output power regardless of body size, implanted location, and organ shape. For example, Wang et al. have reported a ZnO nanowire-based nanogenerator device, which can be driven by ultrasound to produce continuous direct-current output for bio-implantable application [9].

The surfaces of organs in human body such as lung, brain, eye, and heart are always concave-convex. Conventional bio-implantable energy harvesting devices are mostly rigid; hence they are limited for such organs inside human body due to incongruent contact with the corrugated and curved surfaces of the organs [7,10,11]. In order to solve this problem, recent efforts have focused on developing flexible piezoelectric energy harvesters that mainly used the organic piezoelectric thin-film or embed piezoelectric ceramic nanoparticles into polymer substrates [6–8,12–17]. The organic piezoelectric films possess good flexibility. However, the polymer piezoelectrets (mainly polyvinylidene fluoride (PVDF) and its copolymer films) are not suitable to serve as

* Corresponding authors.
E-mail addresses: yang610@usc.edu (Y. Yang), nic0400@scu.edu.cn (J. Zhu), yongchen@usc.edu (Y. Chen), qifazhou@usc.edu (Q. Zhou).

https://doi.org/10.1016/j.nanoen.2018.11.052
Received 13 October 2018; Received in revised form 12 November 2018; Accepted 18 November 2018
Available online 22 November 2018

energy harvesters due to their low electromechanical coupling factors (a parameter characterizing the coupling between electrical energy and mechanical energy) and low permittivities [18,19]. Although the piezoelectric ceramic nanoparticles possess superior electromechanical performance and ease of processing [20–23], their piezoelectricity will be greatly reduced when they are embedded into polymer substrates [24,25]. This is attributed to the inhomogeneous distribution of ceramic nanoparticles in the matrix due to agglomeration. Surface modification of ceramic nanoparticles was performed for the homogeneous distribution in polymer matrix [15], but the difficulties mainly lie in the efficient polarization of the prepared composites to address the insulation characteristics of substrates. That is, the ceramic nanoparticles are not effectively polarized as the polarization voltage is mostly applied on the polymer matrix due to the large difference of dielectric constants between ceramic nanoparticles and polymer matrix [26]. The aforementioned shortcomings represent a bottleneck for the development of advanced piezoelectric energy harvesters, especially ultrasonic energy harvesters, which requires a combination of superior conversion efficiency and desirable flexibility to allow them being applied to general complex surfaces.

In this work, a membrane-based flexible piezoelectric ultrasonic energy harvester (PUEH) array was proposed, which enables bio-

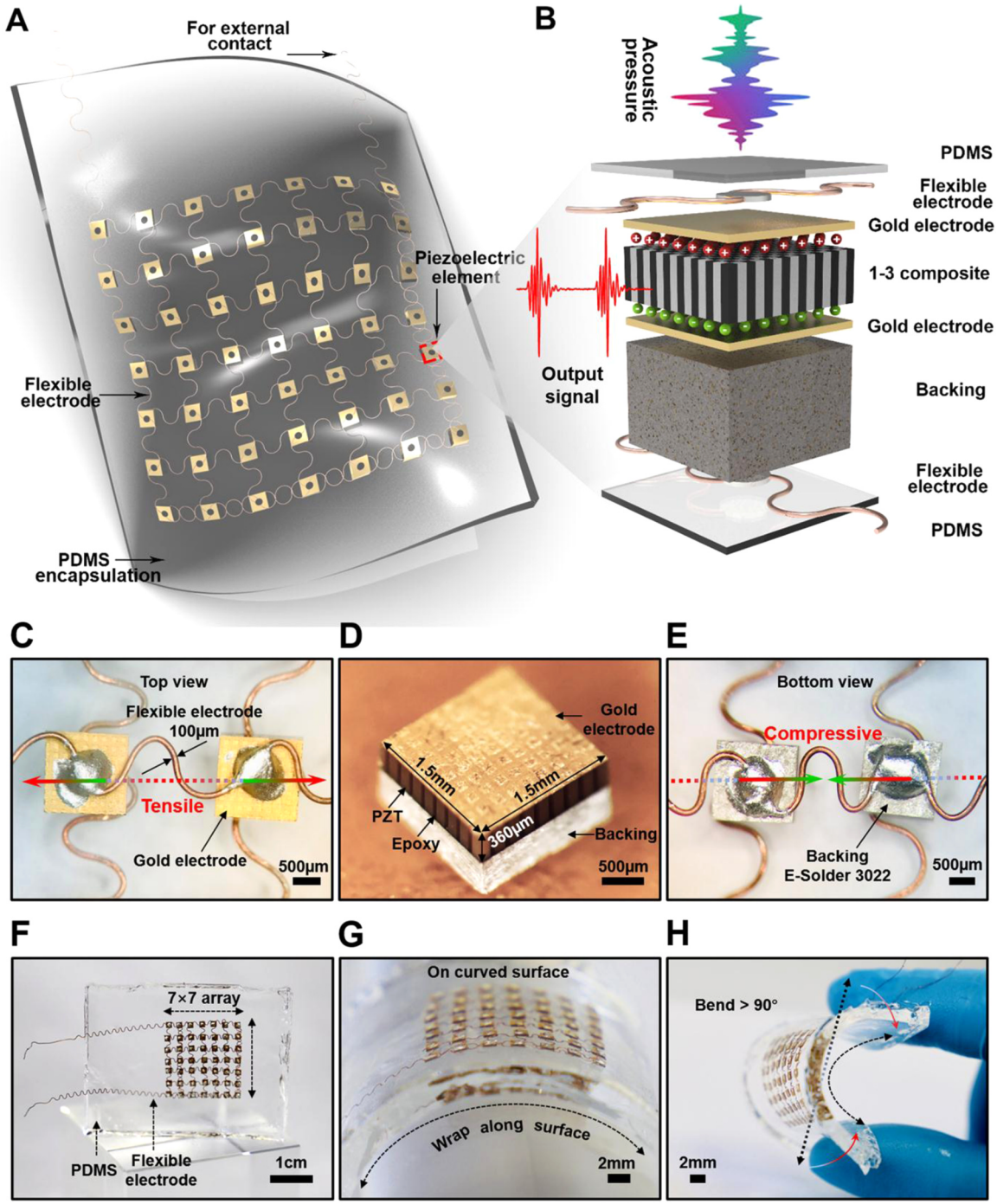

Fig. 1. Schematic and design of the flexible PUEH device. (A) A Schematic to show the device structure. **(B)** Exploded view to illustrate each component in a piezoelectric element. **(C)** The optical image (top view) of two piezoelectric elements. **(D)** The optical image of a 1–3 piezoelectric composite. **(E)** The optical image (bottom view) of two piezoelectric elements. **(F to H)** Optical images of the flexible device when it stands freely, wraps over a curved surface, and bends.

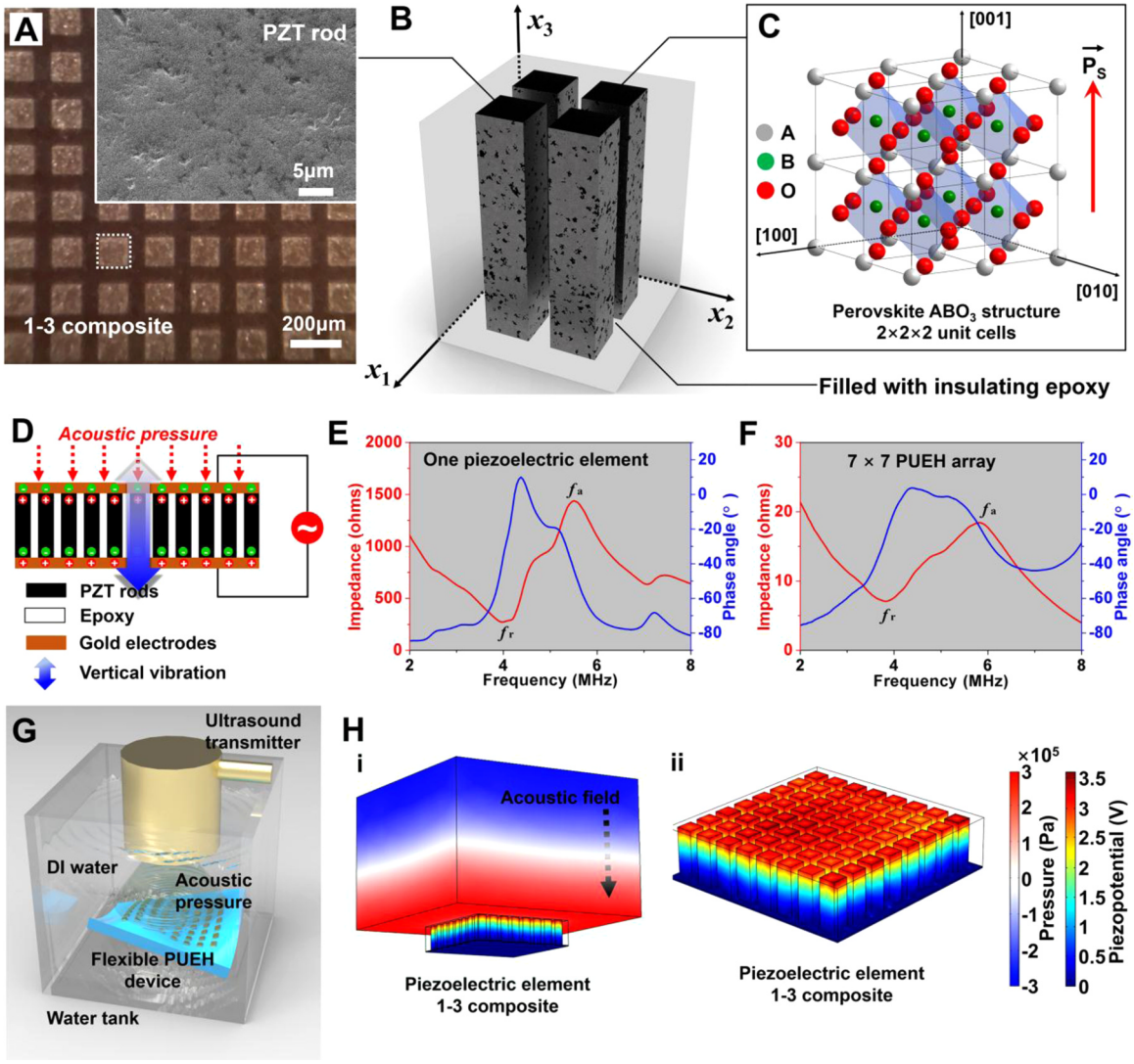

Fig. 2. Characterizations and simulations of the 1–3 composite. (**A**) Optical image of the surface of 1–3 composite; the inset shows the SEM image of a piezoelectric PZT rod. (**B**) Schematic of 1–3 composite. (**C**) Schematic of perovskite ABO_3 structure. (**D**) The vibration schematic of the 1–3 composite. (**E** and **F**) Electrical impedance and phase angle of one piezoelectric element and the 7 × 7 PUEH device. (**G**) Schematic of test setup. (**H**) Simulation results showing the piezoelectric potential distribution inside a composite element driven by acoustic field.

implantable wireless charging via ultrasound and can work effectively on general curved surfaces. The developed device employs an array of thin and high-performance PZT/epoxy 1–3 piezoelectric composites as harvester elements; it also uses double layer wavy copper wires as flexible electrical interconnects and an elastomer membrane as the encapsulation material. Consequently, the piezoelectric elements are effectively polarized and the device keeps flexibility with wavy copper wires. With these unique characteristics, the PUEH device can obtain excellent output signals when working on both planar and curved surfaces. The output voltage, current, power efficiency, etc. of the PUEH device were systematically studied during the energy transfer process. Potential applications of using the PUEH device to charge energy-storage devices and power commercial electronics were also demonstrated. Finally, the in vitro test of the device indicates that the proposed PUEH can serve as a wireless power supply for various bio-implantable systems.

2. Design and analysis

The schematic of the device structure is illustrated in Fig. 1**A**. The piezoelectric elements as the core components for PUEH device are arranged in a 7 × 7 array, connected by a wavy structured matrix of microscale copper wires (the schematic fabrication processes are shown in Fig. S1 in Supplementary material). Although the strain of the components themselves is limited, the wavy bridges can stretch and compress to accommodate the externally applied strain (Fig. 1**C** and **E**). Therefore, the matrix is rigid locally but soft globally. All piezoelectric elements in the matrix are connected in parallel. Fig. 1**B** displays the exploded view of a piezoelectric element. The polydimethylsiloxane (PDMS) elastomer thin films as both the superstrate and substrate offer a compatible platform to accommodate a diverse class of building blocks, such as flexible electrodes, piezoelectric elements, backing layers, and silver paste [27]. The whole thickness of the flexible PUEH device is about 2 mm.

Piezoelectric PZT/epoxy 1–3 composite is selected as the active material of the elements in the energy harvester (Fig. 1**D** and Fig. S2). Compared with the isotropic lead zirconate titanate (PZT) bulk ceramics, the anisotropic 1–3 composites exhibit superior electromechanical coupling factors (longitudinal length mode) that enable the conversion between mechanical energy and electrical energy [28,29]. Conductive silver paste (E-Solder 3022) is chosen as the backing material (Fig. 1**D** and **E**), serving to support and protect the piezoelectric

elements. The conductive silver paste is also used to build robust and electrically conductive piezoelectric elements/flexible metal electrodes interfaces. However, it is very challenging to obtain a flexible array through a traditional electrode to connect a large number of elements.

To successfully connect 49 harvester elements and ensure the flexibility of the device, a wavy electrode design was utilized based on the "helical-structured" method as inspired by Qilin Hua *et al.* for skin-inspired highly stretchable and conformable matrix networks [30]. Multilayered flexible electrodes have also been demonstrated [29,31,32], and this work consists of two layers of wavy electrodes (100 μm in diameter) with intersection in each layer (Fig. 1**C, E** and Fig. S3). All 49 piezoelectric elements are well aligned and distributed into the two layers. Thus, the PUEH array combines the advantages of both 1–3 composites and flexible devices, improving energy conversion efficiency and usability. On one hand, the gap between adjacent harvester elements should be narrow enough to improve the acoustic energy obtained per unit area. On the other hand, enough space between the piezoelectric elements should be assigned to the wavy interconnects for adequate flexibility. Based on the above two factors, a pitch of 3 mm as a preferred size ($1.5 \times 1.5\,mm^2$ element footmark with a gap of 1.5 mm) was adopted in the PUEH array. This pitch design has been validated by our test results. The flexible PUEH array generated considerable output signals (~2 Vpp and ~4 μA) and over 90 degrees bending of the device was achieved. The as-manufactured device is shown in Fig. 1**F-H** and Fig. S4, showing flexible mechanical properties that can be seamlessly bonded on the curved surfaces and achieve a curvature of over 90 degrees. Details of material characterizations and fabrication processes are provided in the Section 5.

3. Results and discussion

The composite material might be superior by combining the desirable properties of two different phases. This concept has proven to be quite useful in designing composite materials composed of PZT and piezoelectrically inactive polymers (refer to the schematic shown in Fig. 2**B**) [28,33,34]. Fig. 2**A** shows the microstructure of the 1–3 composite used in this work, demonstrating a defect-free rod array with uniform periodically ordered structure and dense grain accumulation. The longitudinal ultrasonic waves propagated from the top were received by using the thickness extension mode resonance (Fig. 2**D**). In this mode, the PZT rods in the 1–3 composite vibrate in the fundamental length longitudinal 33 mode with the efficiency determined by the unclamped piezoelectric coupling factor k_{33} [35]. The resonance of the 1–3 composite elements acting as an energy harvesters corresponding to the 33 mode of the PZT rods will be referred to as longitudinal length mode resonance. As illustrated in Fig. 2**E** and **F**, the electrical impedance and phase angle spectra of one piezoelectric element and 7 × 7 PUEH array are measured, respectively, from which the electromechanical coupling factor k (k_{33} and k_{eff}) are evaluated (see Section 5 for details). Accordingly, the k_{33} and k_{eff} are calculated to be ~0.73 and ~0.75, respectively. The bulk PZT has a high d_{33} coefficient as well as a high dielectric constant ε_{33}^{T}. However, isotropic bulk PZT is not an ideal receiver of ultrasound because of the low piezoelectric voltage coefficient g_{33} ($d_{33}/\varepsilon_{33}^{T}$). The benefit of designing a composite harvester allows to improve the g_{33} coefficient as well as to enhance the sensitivity in the receiving mode. With the improvement of the receiving voltage sensitivity, the developed harvester device can work at lower ultrasonic energy with the minimization of the biological effects of ultrasound. The g_{33} coefficient of the composite used in this work is $46.2\,V\,m/N \times 10^{-3}$, which is more than twice that ($19.0\,V\,m/N \times 10^{-3}$) of the bulk PZT-5H material (see Table S1 in Supporting information for the detailed material parameters) [36]. These results indicate the outstanding properties of our energy harvesting device.

According to the design, the PUEH device can be regarded as being composed of parallel-connected oscillator arrays. Under the load of acoustic pressure, all the oscillators vibrate independently along the longitudinal direction. Each oscillator unit can be considered as the current source. The equivalent circuit model for the harvester is shown in Fig. S5. Thus, the total impedance of the harvester Z_t can be determined as:

$$\frac{1}{Z_t} = \sum_{j=1}^{n} \frac{1}{Z_j}, \tag{1}$$

where Z_j is the impedance of the oscillator unit R_j. The calculated result (10–30 Ω) is consistent with the above measured results (Fig. 2**E** and **F**), indicating a good connection of the 49 piezoelectric elements in parallel. The output current I_O and output voltage V_O can be respectively derived as [37,38]:

$$I_O = \sum_{j=1}^{n} I_j = -\frac{P k_{33}^{-2}}{e_{33}} \sum_{j=1}^{n} \frac{h_j}{\xi h_j \cot(\xi h_j)(Z_j + Z_L)}, \tag{2}$$

$$V_O = I_O Z_L = -\frac{P k_{33}^{-2}}{e_{33}} \sum_{j=1}^{n} \frac{h_j Z_L}{\xi h_j \cot(\xi h_j)(Z_j + Z_L)}, \tag{3}$$

where $k_{33}^{-2} = \frac{k_{33}^2}{1+k_{33}^2}$, $k_{33}^2 = \frac{e_{33}^2}{\varepsilon_{33} c_{33}}$, and $\xi^2 = \frac{\rho}{c_{33}(1+k_{33}^2)}\omega^2$. In the above equations, P is the acoustic pressure amplitude applied on the upper surface of the harvester. Z_L is the load. c_{33}, e_{33}, and e_{33} are the effective elastic, piezoelectric, and dielectric constants of the 1–3 piezoelectric composite, respectively. ρ, ω, and ξ are the effective mass density, angular frequency, and wave number, respectively. h_j and S_j are the thickness and area of the oscillator unit R_j, respectively.

To better understand how the device works, a simulation for the piezoelectric potential generated with one element (1–3 composite) placed in the acoustic field is carried out by a finite element analysis (FEA) method using Comsol Multiphysics software, as illustrated in Fig. 2**H**. Since the device is located in the acoustic medium (refer to the schematic shown in Fig. 2**G**), the strain occurs inside the piezoelectric layer during ultrasound propagation. The material parameters required for the simulation are listed in Table S1. The absolute value of piezoelectric potential distribution of 1–3 composite is indicated by the color bar, as shown in Fig. 2**H**. The finite element analysis results show that a 1–3 composite-based PUEH device can convert output piezopotential from ultrasonic energy. The mechanism for the generation of electrical energy from the PUEH device is demonstrated in Fig. 2**D** and **Video S1**, which indicates that piezoelectric composite converts acoustic pressure to an electrical potential. When the 1–3 composite is subjected to the mechanical deformation by an acoustic pressure, the piezoelectric potential is produced between the top and bottom electrodes because of aligned dipoles in the piezoelectric material (Fig. 2**C**). Due to the epoxy in between and the PDMS insulating layers, electrons can flow through the external circuit to balance the field made by the dipoles and accumulate at the interface of the top electrodes [6]. This behavior generates electrical signals of voltage and current. When the 1–3 composite is subjected to reverse acoustic pressure, the strain and the piezoelectric potential are reversed. Subsequently, the accumulated electrons flow back to the bottom electrode through the external circuit, which induces electrical signals in the opposite direction [6].

Supplementary material related to this article can be found online at doi:10.1016/j.nanoen.2018.11.052.

The principle of the PUEH device can be regarded as a hydrophone that converts acoustic signals into electrical signals. Receiving is a non-resonant application: hydrophones work well over the entire band below their resonance point (for our device is ~4 MHz) [39]. In addition to the sensitivity of the PUEH device itself, output signals also depend on the strong acoustic signals generated by the ultrasonic transmitter. To effectively transmit acoustic signals to drive the PUEH device, a low-frequency PZT bulk transducer as the ultrasound transmitter was designed and fabricated, as shown in Fig. S6A. As a transmitter, the bulk transducer can achieve optimum electroacoustic conversion efficiency when operating near its resonant frequency.

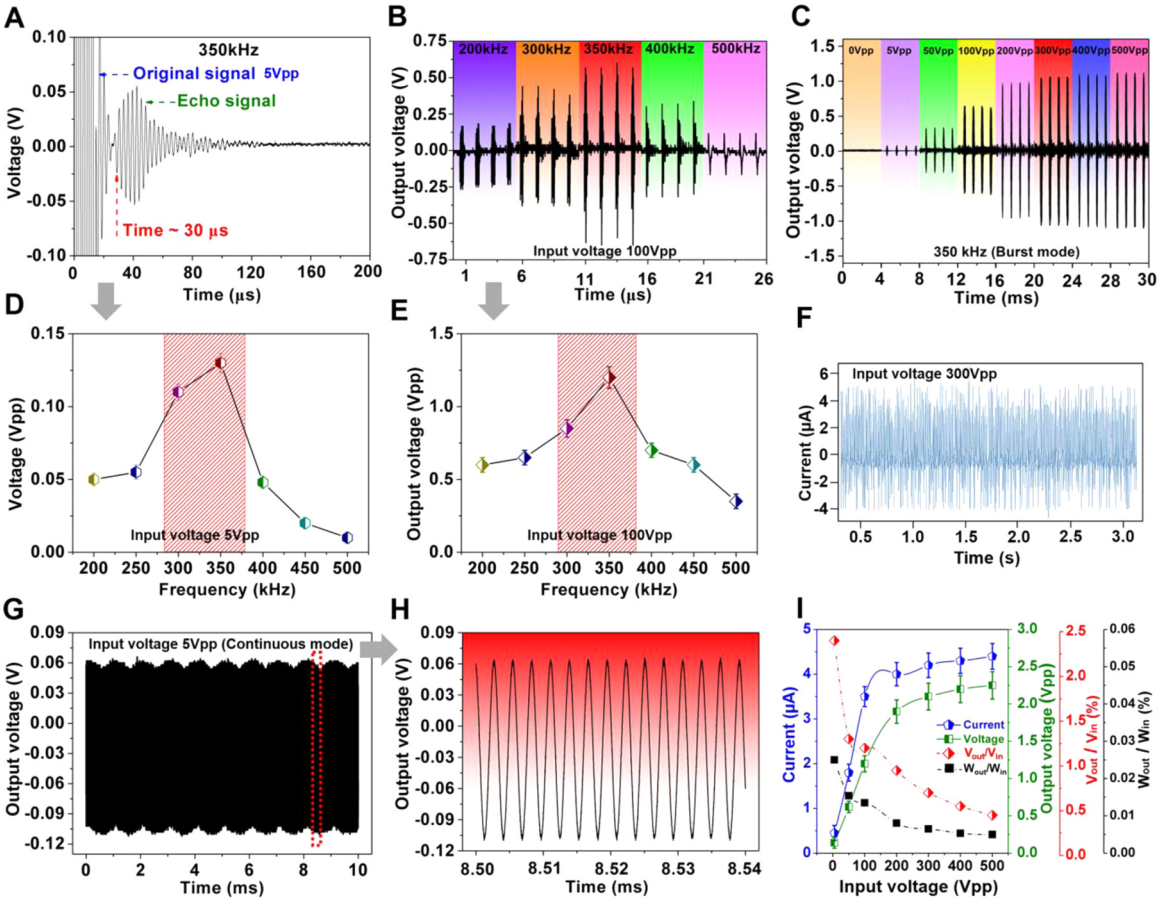

Fig. 3. Characterizations of the output signals. **(A** and **D)** Pulse-echo measurements of the ultrasound transmitter. **(B** and **F)** Output voltage signals of the flexible PUEH device measured at different frequencies. (**C**) Output voltage signals of the flexible PUEH device when the input voltage is from 0 to 500 Vpp in a burst mode. (**E**) Output current signals of the flexible PUEH device when the input voltage is 300 Vpp. (**G** and **H**) Output voltage signal of the flexible PUEH device when the input voltage is 5Vpp in a continuous mode. (**I**) Output current, voltage signals, voltage efficiency, and power efficiency as a function of input voltage, respectively.

According to the impedance spectrum (Fig. S6B) and pulse-echo measurements (Fig. 3**A, D** and Fig. S6C-F) [40,41], the transducer used in this work possesses an optimal working characteristic at the frequency of 200–500 kHz, in which the transmitter can produce strong acoustic signals. Correspondingly, the output signals of the PUEH device driven by the ultrasound were measured over the wide frequency range (200–500 kHz). As demonstrated in Fig. 3**B** and **E**, the PUEH device obtained a maximum output voltage signal (1.2Vpp) at 350 kHz, which is in accordance with the maximum echo signal of the transmitter at 350 kHz. During the measurement, both the transmitter and the PUEH device are immersed in deionized water and the distance between them is fixed to be 23 mm, which can be identified by the time delay (~ 30 μs) of the echo signal [42].

To further investigate the energy harvest characteristics of the PUEH device, we measured the output voltage and current generated from the device under different input power. First, the ultrasonic transmitter transmits 350 kHz ultrasound waves to the PUEH device in a pulsed mode (cycle: 50; trigger interval: 1 ms) (Fig. S7) under different input voltages (from 5 Vpp to 500 Vpp), and the corresponding acoustic intensities were measured by a hydrophone probe (see Section 5 for details). The output signals generated from the PUEH device correspond to a pulse signal and increase with the increment of input voltage, as shown in Fig. 3**C** and Fig. S8. The output signal tends to saturate when the input voltage exceeds 200 V (Fig. 3**C** and **I**). The output signal cannot obtain a significant increase when further increasing the input voltage. In this process, the thermal effects of the device and the cavitation of water caused by ultrasonic waves will increase the loss of transmission energy, resulting in reduced conversion efficiency. When the ultrasonic transmitter was driven by a sinusoidal signal with a voltage of 300 Vpp at the frequency of 350 kHz, the acoustic pressure value was measured to be 44.2 kPa. The corresponding acoustic intensity is about 65 mW/cm^2. In this case, the efficiency was calculated to be about 0.0063% with the output power of the flexible PUEH to be 4.1 μW/cm^2. Although the power efficiency is not high, this wireless energy transmission system is still effective to generate considerable values of output voltage (2.1 Vpp) and current (4.2 μA). The results indicate that the flexible PUEH device can compete with other bulk ultrasonic energy harvesters (see Table S2 and Fig. S9) [9,10,43–48], even with some traditional mechanical vibration energy harvesters [6,8,49–51]. To further confirm that the obtained output signals are purely introduced by the piezoelectric effect of the PUEH array, a continuous 5 Vpp 350 kHz sinusoidal signal was switched to drive the ultrasonic transmitter. Correspondingly, the measured output signal generated from the PUEH device is a continuous sinusoidal signal (Fig. 3**G** and **H**). Furthermore, we have characterized that no reliable signals were observed by using pure PDMS polymer without piezoelectric elements, as shown in Fig. S10. The result indicates that the output signals are obtained from charges generated by piezoelectric material in the array during the ultrasound propagation induced vibration.

As an ultrasonic energy harvester with superior output performance, the as-fabricated PUEH device is capable of acting as a wireless power supply. For a potential utilization of our energy harvesting technology, the lighting up of commercial light-emitting diodes (LEDs) was demonstrated using the electricity generated from the PUEH device. To implement the energy rectification and storage process of the generated

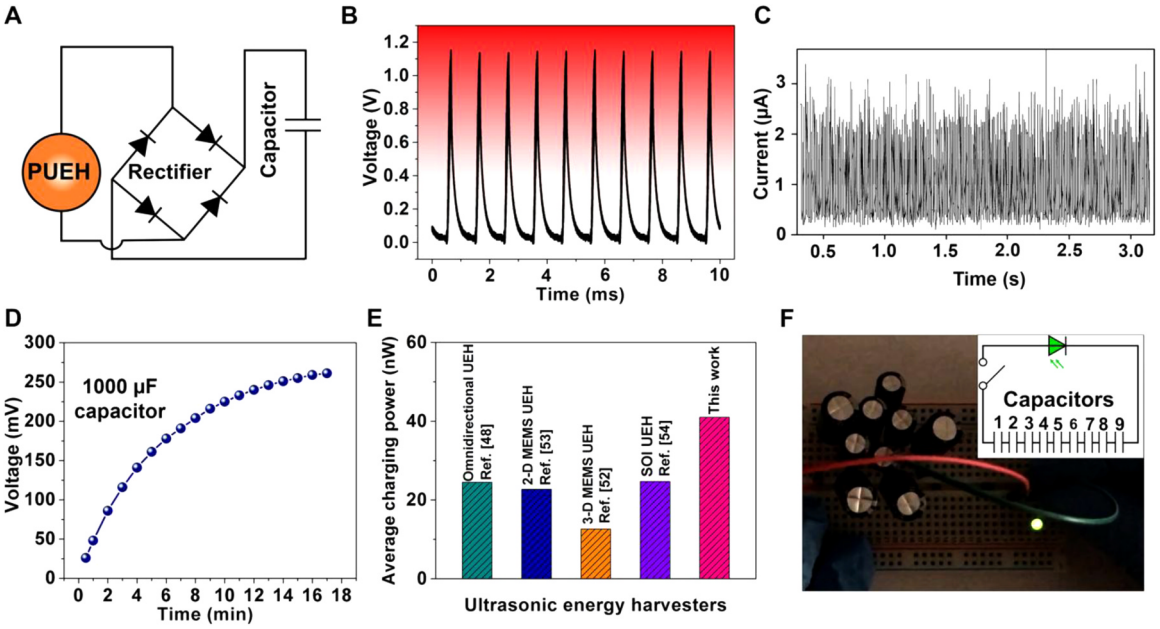

Fig. 4. Applications of the flexible PUEH device. (A) Schematic design diagram of the energy rectifier and storage circuit comprising four diodes and one capacitor. (**B** and **C**) Output voltage and current signals after rectification, respectively. (**D**) The charging time dependence of voltage in the storage capacitor. (**E**) Comparison of the average charging power of ultrasonic energy harvesters. (**F**) Optical image showing a commercial green LED lit up by the energy stored in capacitors; the inset shows the schematic circuit diagram of nine capacitors in serial.

alternating output signals, the PUEH device was incorporated into a predesigned circuit shown in Fig. 4**A**. The rectified output signals (Fig. 4**B** and **C**) using a full-wave bridge rectifier consisting of four diodes were stored by a 1000 μF capacitor. During the charging process, the voltage stored in the capacitor increased to be 270–290 mV, which was obtained through receiving the pulsed ultrasound for about 15 min (Fig. 4**D** and Fig. S11A). The average charging power $\bar{P}_C$ harvested by the device was determined via the method, which is given by [52]

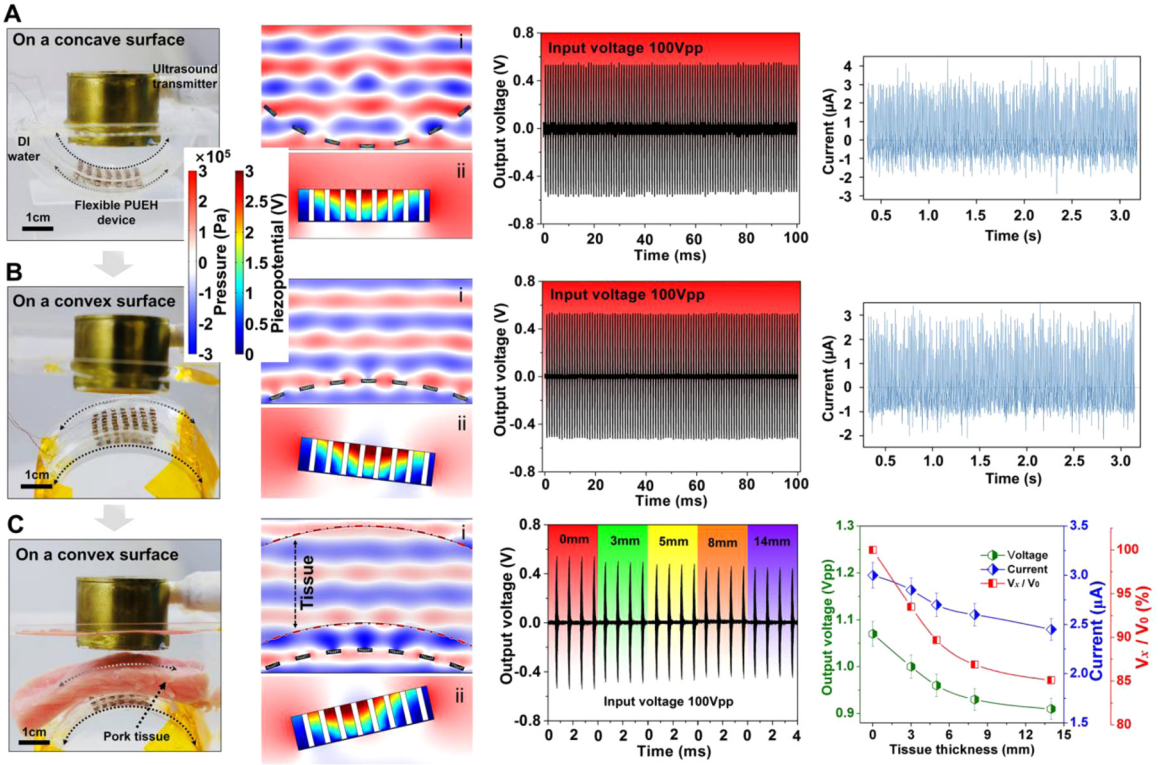

Fig. 5. Simulations and characterizations of the PUEH device when the device is on concave-convex surfaces to mimicked in implanted situations. Optical images of experimental setups with the flexible PUEH device tested on (A) concave surface, (B) convex surface, and (C) convex surface where pork tissue inserted between the transmitter and the PUEH device to mimic the implanted situation (first column); simulation results in different situations (second column); Output voltage and current signals measured in different situations (third and fourth columns). V_x/V_0, the ratio of output voltages with and without the presence of pork tissue.

$$\bar{P}_C = \frac{1}{2} C_S V^2, \tag{4}$$

where C_S is the capacitance of the storage capacitor, V is the final voltage on the capacitor and T is the period over which the power is calculated. Based on these measurements, the electrical power harvested by the PUEH device was calculated to be about 40 nW, which is larger than previously reported results (~ 20 nW) of ultrasonic energy harvester (UEH) via this method (Fig. 4**E**) [48,52–54]. The voltage charged to a single capacitor is lower than the peak value of output voltage because of the low valid value of a pulse sinusoidal signal and the capacitor leakage [8,55]. In the same way, we charged nine identical capacitors separately. By connecting the nine charged capacitors in series, the total usable voltage was increased to be 2.13 V (Fig. S11B), which is enough to light up a commercial LED. To verify this hypothesis, a commercial LED and nine capacitors in series were integrated into a predesigned circuit demonstrated in Fig. 4**F** (inset). When the switch is turned on, the electric power produced from the ultrasonic energy was successfully applied to light up a commercial green LED (Fig. 4**F**). Then, the remaining electricity after lighting up the green LED was used to drive a commercial white LED, which was also lit up and lasted more than 3 s (Fig. S11C) (see **Video S2** in Supporting information for video clips of the LEDs being lit up by the electric power generated from the PUEH device). As a conclusion, the commercial microelectronic LEDs were successfully operated by electricity from the PUEH device without any external electric power sources. The results demonstrate the potential application of the PUEH device as a wireless power supply.

Supplementary material related to this article can be found online at doi:10.1016/j.nanoen.2018.11.052.

For the wearable and bio-implantable applications of the wireless power supply, perfect fit for complex surfaces requires flexible mechanical properties. Here we studied the output performance by laminating seamlessly the flexible PUEH device on both concave and convex surfaces (Fig. 5**A** and **B**, first column). As indicated by the acoustic field simulation results, piezoelectric elements at different latitudes on curved surfaces are located in different acoustic pressure levels in the acoustic field (Fig. 5**A** and **B**, second column). Each piezoelectric element of the PUEH device produces an inconstant or even opposite piezoelectric potential, depending on its position in the acoustic field. Consequently, the output performance of the PUEH device may be greatly reduced in the connection of elements in parallel. In this work, a 3D-axis motor system was used to adjust the direction of the ultrasonic emission and the distance between the transmitter and the receiver to optimize the output performance. The generated voltage and current signals of the PUEH device are 1.12 Vpp, 3.1 μA, and 1.07 Vpp, 2.9 μA for concave and convex surfaces, respectively (Fig. 5**A** and **B,** third and fourth columns). These results show that the flexible PUEH device is capable of working on concave-convex surfaces and providing excellent output signals.

Finally, in vitro test of the flexible PUEH device to transmit power through a pork tissue is performed. Fig. 5**C** and Fig. S12 show the experimental setup, simulation and test results, in which different thicknesses of pork tissue are inserted between the transmitter and the PUEH device to mimic the different depth in the implanted tissue. The output signals do not show a significant decrease when the thickness of the inserted pork tissue increases from 0 mm to 14 mm. When the inserted pork tissue reaches a thickness of 14 mm, the generated voltage is 0.91 Vpp, which is 85% of the value (1.07 Vpp) without the presence of pork tissue. The correspondingly generated current signals are 3 μA and 2.5 μA, respectively. As far as we know, there is acoustic reflection at the interface and acoustic absorption through the medium (mainly converted to heat) during ultrasonic propagation due to the impedance mismatch between the tissue (~ 1.70 MRayl) and the aqueous medium (~ 1.50 MRayl), thereby reducing the ultrasound energy [56]. The following formula is used to compute the frequency dependent attenuation [57]:

$$A(\omega) \cong [A_0(\omega) - A_f(\omega)] \cdot e^{-\alpha(\omega) \cdot l}, \tag{5}$$

where $A_f(\omega)$ represents the part of the reflected signal which does not pass through the tissue, l is the thickness of tissue, and $\alpha(\omega)$ is the frequency dependent acoustic absorption coefficient defined by Stokes-Kherhoff formula [58]:

$$\alpha(\omega) = \frac{\omega^2}{2\rho_0 c^3}\left[\frac{4}{3}\eta' + \chi\left(\frac{1}{C_V} - \frac{1}{C_P}\right)\right]. \tag{6}$$

In the above equations, ρ_0 is density, c is acoustic velocity, ω is frequency, η' is shear viscosity coefficient, χ is heat transfer coefficient, C_P is constant pressure specific heat capacity, and C_V is constant volume heat capacity. According to the parameters of pork lion tissue, the calculated acoustic absorption coefficient α is about 5.5 m^{-1} when the frequency of ultrasound is 1 MHz, indicating that the attenuation through the 14 mm pork tissue will be less than 8% when the frequency used is below 1 MHz [59]. This conclusion is roughly in accordance with the experimental results when considering the reflection portion. The proposed flexible PUEH device is capable of harvesting energy even imbedded in biological tissues, and thus can be adopted as a wireless power supply for various bio-implantable systems, such as high-density neural stimulation, cardioverter defibrillators, pacemakers, etc. [1–3].

4. Conclusion

In summary, we have designed and fabricated a flexible piezoelectric ultrasonic energy harvester (PUEH), which exploits a 7 × 7 array of thin and high-performance 1–3 piezoelectric composite as active elements, and uses multilayered flexible electrodes as electrical interconnects and an elastomer membrane (PDMS) as the encapsulating material. The PUEH device can provide continuous power output through an ultrasonic energy source. The output voltage and current signals generated from the PUEH device reach 2.1 Vpp and 4.2 μA, respectively, showing higher output performance than those of the previously reported ultrasonic energy harvesters. The generated electricity can be stored in capacitors and successfully used to light up commercial LEDs without an external power source. The flexible device fits perfectly on curved surfaces and still maintains an excellent output performance. Additionally, in the in vitro test, output signals exhibit weak attenuation performance (~ 15%) when the mimicked implanted tissue reaches the thickness of 14 mm. Therefore, our fabricated 1–3 composite-based PUEH array is a significant breakthrough in the flexible ultrasound energy harvesting field, showing great potential in the next generation of wirelessly powered bio-implantable micro-devices.

5. Experimental section

5.1. Fabrication of the flexible electrodes

Flexible electrodes as electrical interconnects are a unique design in this study. The design and fabrication are shown in Fig. S3. First, a 100 μm diameter copper wire was wrapped equidistantly around an 800 μm diameter brass rod by using a lathe (SD 400, PRAZI). Then, we removed the “helical-structured” copper wire from the brass rod and laid it flat on the water platform. After that, a polished flat ingot was used to press the straight spring-like copper wire into a flat plane to obtain the flat wavy electrodes. Finally, these wavy copper wires were linked together with solder paste to serve as the top and bottom flexible electrodes of the PUEH device.

5.2. Assembling of PUEH array and its integration with electrodes

As demonstrated in Fig. S1, the process began with the fabrication of the backing layer after Cr/Au (50/100 nm) electrodes (NSC-3000

Sputter Coater, Nano-Master, Inc., Austin, TX, USA) have been sprayed on both sides of the piezoelectric 1–3 composite (Del Piezo Specialties, LLC). The size of each PZT pillar of the 1–3 composite was $120 \times 120\ \mu m^2$ with a kerf of 60 μm (Fig. 2**A** and Fig. S2B). The conductive backing material was fabricated by mixing a silver-epoxy composite (E-Solder 3022, Von Roll Isola, New Haven, CT, USA) with a hardener Insulcure 9 (American Safety Technologies, Roseland, NJ) in a 10:0.8 ratio and then curing on the bottom side of the composite. After curing at 40 ℃ for 4 h, the backing was lapped down to about 400 μm thick. Then the whole acoustic stack was diced into small posts with aperture size of $1.5 \times 1.5\ mm^2$ by a dicing saw (Tcar 864–1, Thermocarbon, Casselberry, FL, USA). Both the top and bottom flexible electrodes were bonded with the 7×7 arrayed acoustic posts by conductive silver paste ((E-Solder 3022) cured in an oven at 40 ℃ for 4 h. The gap between the sandwiched device was then filled using PDMS (Sylgard 184, Dow Corning, Corp.) and cured at 60 ℃ for 4 h. Afterward, the plastic slides were removed, yielding a freestanding flexible piezoelectric ultrasonic energy harvester (Fig. 1**F**).

5.3. Characterizations and measurements

Impedance spectrums (Fig. 2**E** and **F**) of the 1–3 composite and PUEH array were characterized by an impedance analyzer (4294A, Agilent). According to the IEEE standard on piezoelectricity [60], the electromechanical coupling factor, k_{33} (longitudinal length mode electromechanical coupling factor of a material) and k_{eff} (effective electromechanical coupling factor of a device), describing the conversion efficiency between mechanical energy and electrical energy, were determined by

$$k_{33} = \sqrt{\frac{\pi}{2}\frac{f_r}{f_a}\tan\left(\frac{\pi}{2}\frac{f_a - f_r}{f_a}\right)}, \tag{7}$$

$$k_{eff} = \sqrt{1 - \frac{f_r^2}{f_a^2}}, \tag{8}$$

where the f_r and f_a are the resonant frequency and anti-resonant frequency, respectively. The capacitance and dielectric loss were measured by an inductance-capacitance-resistance (LCR) digital bridge machine (QuadTech, Inc.). A summary of some important acoustic and piezoelectric properties of the composite is shown in Table S1.

The Output signals of the PUEH device were measured by a multifunctional setup (Fig. S13). A bulk PZT transducer as the ultrasonic transmitter was mounted on a 3D-axis holder (OptoSigma, Corp.) and immersed in a tank filled with deionized water. The PUEH device was placed about 23 mm away from the transmitter as a receiver. The transmitter was triggered by an input sinusoidal signal, which was given by a function generator (AFG3252C, Tektronix) and then amplified by an amplifier (75A250A, Amplifier Research). The output voltage and current signals generated from the PUEH device were measured by a digital oscilloscope (TDS 5052, Tektronix) with an internal impedance of 1 MΩ and a source measurement unit (2400, Keithley), respectively. The acoustic pressure output of the ultrasonic transmitter has been measured in the water tank with a hydrophone probe (HGL-1000, ONDA, Inc.) placed at 23 mm distal to the ultrasonic transmitter. Acoustic intensity can be calculated from the measured pressure by the following equation [10]:

$$I = \frac{P^2}{2Z}, \tag{9}$$

where I is the acoustic intensity, P is the acoustic pressure and Z is the acoustic impedance (for aqueous medium, Z is about 1.50 MRayl).

Acknowledgements

This work was partially supported by the National Institutes of Health (NIH) under grant 1R01EY026091, R01 EY028662 and R01 HL127271, the National Science Foundation (NSF) under grant CMMI 1335476 and CMMI 1663663, and an UNRESTRICTED GRANT to the Department of Ophthalmology from Research to Prevent Blindness, New York, NY. The work of L. Jiang was supported by the China Scholarship Council (File no.: 201706240056).

Conflict of interest

The authors declare no conflict of interest.

Appendix A. Supporting information

Supplementary data associated with this article can be found in the online version at doi:10.1016/j.nanoen.2018.11.052

References

[1] E. Meng, R. Sheybani, Lab Chip 14 (2014) 3233–3240.
[2] W. Mokwa, Meas. Sci. Technol. 18 (2007) R47.
[3] D. Rodger, A. Fong, W. Li, H. Ameri, A. Ahuja, C. Gutierrez, I. Lavrov, H. Zhong, P. Menon, E. Meng, Sens. Actuators B: Chem. 132 (2008) 449–460.
[4] F.W. Horlbeck, F. Mellert, J. Kreuz, G. Nickenig, J.O. Schwab, J. Cardiovasc. Electrophysiol. 23 (2012) 1336–1342.
[5] V.S. Mallela, V. Ilankumaran, N.S. Rao, Indian Pacing Electrophysiol. J. 4 (2004) 201.
[6] K.-I. Park, C.K. Jeong, J. Ryu, G.-T. Hwang, K.J. Lee, Adv. Energy Mater. 3 (2013) 1539–1544.
[7] G.T. Hwang, M. Byun, C.K. Jeong, K.J. Lee, Adv. Healthc. Mater. 4 (2015) 646–658.
[8] K.I. Park, M. Lee, Y. Liu, S. Moon, G.T. Hwang, G. Zhu, J.E. Kim, S.O. Kim, D.K. Kim, Z.L. Wang, Adv. Mater. 24 (2012) 2999–3004.
[9] X. Wang, J. Song, J. Liu, Z.L. Wang, Science 316 (2007) 102–105.
[10] Q. Shi, T. Wang, C. Lee, Sci. Rep. 6 (2016) 24946.
[11] W.-S. Jung, M.-J. Lee, M.-G. Kang, H.G. Moon, S.-J. Yoon, S.-H. Baek, C.-Y. Kang, Nano Energy 13 (2015) 174–181.
[12] W.-S. Jung, M. Lee, S.-H. Baek, I.K. Jung, S.-J. Yoon, C.-Y. Kang, Nano Energy 22 (2016) 514–523.
[13] X. Lu, H. Qu, M. Skorobogatiy, Sci. Rep. 7 (2017) 2907.
[14] K.I. Park, S. Xu, Y. Liu, G.T. Hwang, S.J. Kang, Z.L. Wang, K.J. Lee, Nano Lett. 10 (2010) 4939–4943.
[15] E.J. Lee, T.Y. Kim, S.-W. Kim, S. Jeong, Y. Choi, S.Y. Lee, Energy Environ. Sci. 11 (2018) 1425–1430.
[16] G. Zhang, P. Zhao, X. Zhang, K. Han, T. Zhao, Y. Zhang, C.K. Jeong, S. Jiang, S. Zhang, Q. Wang, Energy Environ. Sci. 11 (2018) 2046–2056.
[17] S. Xu, Y. Qin, C. Xu, Y. Wei, R. Yang, Z.L. Wang, Nat. Nanotechnol. 5 (2010) 366–373.
[18] D. Powell, G. Hayward, IEEE transactions on Ultrasonics, Ferroelectrics, and Frequency Control, 43, 1996, pp. 393–402.
[19] Y. Qi, N.T. Jafferis, K. Lyons Jr., C.M. Lee, H. Ahmad, M.C. McAlpine, Nano Lett. 10 (2010) 524–528.
[20] L. Jiang, J. Xing, Z. Tan, J. Wu, Q. Chen, D. Xiao, J. Zhu, J. Mater. Sci. 51 (2016) 4963–4972.
[21] J. Xing, Z. Tan, L. Jiang, Q. Chen, J. Wu, W. Zhang, D. Xiao, J. Zhu, J. Appl. Phys. 119 (2016) 034101.
[22] L. Jiang, Z. Tan, L. Xie, Y. Li, J. Xing, J. Wu, Q. Chen, D. Xiao, J. Zhu, J. Eur. Ceram. Soc. 38 (2018) 2335–2343.
[23] Z. Chen, X. Song, L. Lei, X. Chen, C. Fei, C.T. Chiu, X. Qian, T. Ma, Y. Yang, K. Shung, Y. Chen, Q. Zhou, Nano Energy 27 (2016) 78–86.
[24] Z. Li, D. Zhang, K. Wu, J. Am. Ceram. Soc. 85 (2002) 305–313.
[25] S.-Y. Fu, X.-Q. Feng, B. Lauke, Y.-W. Mai, Compos. Part B: Eng. 39 (2008) 933–961.
[26] Y. Yang, H. Sun, D. Yin, Z. Lu, J. Wei, R. Xiong, J. Shi, Z. Wang, Z. Liu, Q. Lei, J. Mater. Chem. A 3 (2015) 4916–4921.
[27] B.-H. Jo, L.M. Van Lerberghe, K.M. Motsegood, D.J. Beebe, J. Micro. Syst. 9 (2000) 76–81.
[28] T.R. Gururaja, W.A. Schulze, L.E. Cross, R.E. Newnham, B.A. Auld, Y.J. Wang, IEEE Trans. Sonics Ultrason. 32 (1985) 481–498.
[29] H. Hu, X. Zhu, C. Wang, L. Zhang, X. Li, S. Lee, Z. Huang, R. Chen, Z. Chen, C. Wang, Sci. Adv. 4 (2018) eaar3979.
[30] Q. Hua, J. Sun, H. Liu, R. Bao, R. Yu, J. Zhai, C. Pan, Z.L. Wang, Nat. Commun. 9 (2018) 244.
[31] L. Guo, S.P. DeWeerth, Adv. Mater. 22 (2010) 4030–4033.
[32] S. Xu, Y. Zhang, J. Cho, J. Lee, X. Huang, L. Jia, J.A. Fan, Y. Su, J. Su, H. Zhang, H. Cheng, B. Lu, C. Yu, C. Chuang, T.I. Kim, T. Song, K. Shigeta, S. Kang, C. Dagdeviren, I. Petrov, P.V. Braun, Y. Huang, U. Paik, J.A. Rogers, Nat. Commun. 4 (2013) 1543.
[33] H.L.W. Chan, J. Unsworth, IEEE Transactions on Ultrasonics, Ferroelectrics, and Frequency Control, 36, 1989, pp. 434–441.
[34] Z. Yang, H. Wang, C. Zhao, D. Zeng, Philos. Mag. Lett. 95 (2015) 324–332.
[35] D.A. Berlincourt, D.R. Curran, H. Jaffe, Phys. Acoust.: Princ. Methods 1 (1964) 247.
[36] R.E. McKeighen, Design guidelines for medical ultrasonic arrays, in: K.K. Shung (Ed.

) Ultrasonic Transducer Engineering: Medical Imaging, 1998, pp. 2–18.
[37] Z. Yang, D. Zeng, H. Wang, C. Zhao, J. Tan, Smart Mater. Struct. 24 (2015) 075029.
[38] Y. Sun, X. Gao, H. Wang, Z. Chen, Z. Yang, Appl. Phys. Lett. 112 (2018) 043903.
[39] L. Ivey, NRL-USRD series F42 omnidirectional standard transducers, Naval Research Laboratory, Underwater Sound Reference Detachment, 1979.
[40] K.K. Shung, M. Zippuro, IEEE Eng. Med. Biol. Mag. 15 (1996) 20–30.
[41] K.K. Shung, J. Cannata, Q. Zhou, J. Electroceram. 19 (2007) 141–147.
[42] K.K. Shung, J. Med. Ultrasound 17 (2009) 25–30.
[43] T. Ishiyama, Y. Kanai, J. Ohwaki, M. Mino, Ultrasonics IEEE Symposium on, IEEE, 2003, pp. 1368–1371.
[44] Q. Shi, T. Wang, T. Kobayashi, C. Lee, Micro electro mechanical systems (MEMS), in: IEEE Proceedings of the 29th International Conference on, IEEE, 2016, pp. 1256–1259.
[45] Q. He, J. Liu, B. Yang, X. Wang, X. Chen, C. Yang, Sens. Actuators A: Phys. 219 (2014) 65–72.
[46] B.-S. Lee, P.-J. Shih, J.-J. He, W.-P. Shih, W.-J. Wu, Sensor systems and networks: phenomena, technology, and applications for NDE and health monitoring, in: International Society for Optics and Photonics, 2007, p. 65300I.
[47] Y. Zhu, S. Moheimani, M. Yuce, IEEE Electron Device Lett. 31 (2010) 374–376.
[48] A.G. Fowler, S. Moheimani, S. Behrens, J. Micro. Syst. 23 (2014) 1454–1462.
[49] J. Wu, H. Shi, T. Zhao, Y. Yu, S. Dong, Adv. Funct. Mater. 26 (2016) 7186–7194.
[50] C.R. Bowen, H.A. Kim, P.M. Weaver, S. Dunn, Energy Environ. Sci. 7 (2014) 25–44.
[51] K. Li, Q. He, J. Wang, Z. Zhou, X. Li, Microsyst. Nanoeng. 4 (2018).
[52] A.G. Fowler, S.R. Moheimani, S. Behrens, Sensors IEEE, 2012, pp. 1–4.
[53] Z. Yong, S.O.R. Moheimani, M.R. Yuce, IEEE Sens. J. 11 (2011) 155–161.
[54] A.G. Fowler, S.O.R. Moheimani, S. Behrens, J. Phys.: Conf. Ser. 476 (2013) 012002.
[55] G. Zhu, R. Yang, S. Wang, Z.L. Wang, Nano Lett. 10 (2010) 3151–3155.
[56] F. d'Astous, F. Foster, Ultrasound Med. Biol. 12 (1986) 795–808.
[57] S. Chaffaı, F. Padilla, G. Berger, P. Laugier, J. Acoust. Soc. Am. 108 (2000) 1281–1289.
[58] W.J. Fry, R.B. Fry, J. Acoust. Soc. Am. 26 (1954) 294–310.
[59] K.W. Nowak, Technical Sciences/University of Warmia and Mazury in Olsztyn, 2015, pp. 79–84.
[60] T.R. Meeker, IEEE Transactions on Ultrasonics Ferroelectrics and Frequency Control, 43, 1996, pp. 717–718.